Scattering of Nitrogen Atoms off Ag(111) Surfaces: A Theoretical Study

L. Martin-Gondre,[*,†,‡,¶] G. A. Bocan,[§,⊥] M. Blanco-Rey,[†] M. Alducin,[†,‡] J. I. Juaristi,[†,‡,‖] and R. Díez Muiño[†,‡]

Donostia International Physics Center, Paseo Manuel de Lardizábal 4, 20018 Donostia-San Sebastián, Spain, Centro de Física de Materiales CFM/MPC (CSIC-UPV/EHU), Paseo Manuel de Lardizábal 5, 20018 Donostia-San Sebastián, Spain, Institut des Sciences Moléculaires, UMR 5255 CNRS - Université Bordeaux 1, 351 Cours de la Libération, 33405 Talence Cedex, France, CONICET and Centro Atómico Bariloche (CNEA), Av. Bustillo 9500, 8400 S.C. de Bariloche, Argentina, and Departamento de Física de Materiales, Facultad de Químicas UPV/EHU, Apartado 1072, 20018 Donostia-San Sebastián, Spain

E-mail: lu.martin@ism.u-bordeaux1.fr

Phone: +33 0540003464 . Fax: +33 0540008402

[*]To whom correspondence should be addressed

[†] Donostia International Physics Center, Paseo Manuel de Lardizábal 4, 20018 Donostia-San Sebastián, Spain

[‡] Centro de Física de Materiales CFM/MPC (CSIC-UPV/EHU), Paseo Manuel de Lardizábal 5, 20018 Donostia-San Sebastián, Spain

[¶] Institut des Sciences Moléculaires, UMR 5255 CNRS - Université Bordeaux 1, 351 Cours de la Libération, 33405 Talence Cedex, France

[§] CONICET and Centro Atómico Bariloche (CNEA), Av. Bustillo 9500, 8400 S.C. de Bariloche, Argentina

[‖] Departamento de Física de Materiales, Facultad de Químicas UPV/EHU, Apartado 1072, 20018 Donostia-San Sebastián, Spain

[⊥]Dr. Bocan's affiliation during part of this work was Donostia International Physics Center DIPC, San Sebastián, Spain.

Abstract

The study of the reflection of N atoms on a Ag(111) surface is performed by means of classical molecular dynamics and using an accurate three-dimensional potential energy surface, built from density functional theory calculations. The influence of energy loss channels is analyzed by including phonon and electron-hole pair excitations in the simulations. Our calculations show good agreement with recent experimental results. The broadness of the experimental angular distributions is due to the corrugation of the potential energy surface and is well reproduced by our model. Regarding the energy loss distributions, we show that the simulation of an effusive beam coupled to phonon excitations is required to obtain satisfactory results. This is due to dynamic effects that make the reflection process very dependent on the initial energy of N atoms.

Keywords: Gas/surface; Classical dynamics; Inelastic scattering; Phonons excitations; Electron-hole pair excitations; Effusive atomic beam

Introduction

The study of the dynamical interaction between model metal surfaces and gas phase species (either neutral or ionic, atomic or molecular) is closely connected to the quest for systems where reactivity is enhanced.[1] The ability of a surface to facilitate molecular bond breaking is dictated by two main factors: (i) the corrugated topography of the potential energy surface (PES) of the gas phase species as a function of its spatial coordinates as it approaches the surface, which is an adiabatic interaction; and (ii) the non-adiabatic effects that result in an energy exchange with the surface. These energy dissipation channels follow from electron-hole (*e*-*h*) pair excitation and interaction with the vibrating surface lattice (phonons). The use of *ab-initio* calculations based on density functional theory (DFT) allows for the construction of highly accurate multidimensional PES, which can be used as input for molecular dynamics (MD) simulations. This procedure has turned out to be a robust tool in the understanding of the dynamics of atoms and diatomic

molecules impinging on metal surfaces, as it provides quantitative values for the initial sticking probabilities, angular distributions of the reflected species, activation energies, etc.[2–5] These magnitudes are directly comparable to their experimental counterparts, which are typically obtained in molecular beam experiments. There are recent examples in the literature where the interplay of multidimensional and non-adiabatic effects has been assessed using these methodologies.[6–12] In the present paper, we have used these techniques to obtain an accurate theoretical description of the N-Ag(111) interaction by means of a full three-dimensional adiabatic PES, constructed from *ab-initio* data and an elaborate interpolation method.[13] The two types of aforementioned energy loss channels are accounted for later, within classical MD simulations.

Typically, the PES topography is intricate, and depends strongly on the surface structure and the atomic species involved. Furthermore, the use of vibrationally excited,[14–16] or hyperthermal molecules provides access to vaster regions of the configuration space in a beam experiment. Dynamical studies of this kind yield valuable information on the surface reactivity. N_2 dissociation is a prototype in dynamical studies due to its relevance for ammonia synthesis. It is quite an inert molecule as 9.8 eV are needed to break its triple bond in the gas phase. However, the activation energy can be considerably reduced when N_2 dissociates on metal surfaces.[17–27]

Interestingly, Ag(111) seems to be a fairly inactive surface towards N_2. For example, molecular beam experiments with N_2 molecules of large kinetic energies, 5.6 eV in average, show that scattering is nearly specular, consistent with the picture of a repulsive molecule-surface interaction.[28,29] Interaction with atomic N poses a completely different scenario. N strongly interacts with metals due to its open shell nature. In fact, N atoms chemisorb on Ag(111) with a binding energy of 2.03 eV (per atom),[30] and recombination of chemisorbed atoms into N_2 is relevant.[31] Therefore, significant charge exchange with the surface is foreseen that would result in remarkable non-adiabatic effects. No signal of continuous N uptake is observed, and coverage beyond saturation results in the recombination of atoms as N_2.[31] Thus, the presence of nitrides can be ruled out on this surface. On Cu(111), however, N binds strongly (3.78 eV per atom in the low coverage limit) and surface reconstruction and nitride formation is anticipated.[32]

Beams experiments employing hyperthermal atomic projectiles and metal substrates are scarce, specially for atoms as large as N. Traditionally, these experiments have used light atoms and have been focused in the problem of molecule formation via Eley-Rideal mechanisms, i.e. surface atom pick up by an atomic projectile. For example, beams of H and D have been dosed on Cl-covered Au(111)[33,34] and H-covered Cu(111),[35] respectively. The study of the scattering of open-shelled heavier atoms is motivated by the need of understanding the extent to which the energy loss mechanisms influence the dynamics of a number of events that occur while a surface probing experiment is conducted, such as adsorption, intake and surface diffusion of individual atoms. With this aim, molecular beam experiments were carried out recently by Ueta *et al.* on the scattering of N atoms off Ag(111) at average kinetic energies $< E_i^T >= 4.3\,\text{eV}$.[36] Scattering of N atoms off N-covered Ag(111) surfaces has also been measured[29] and analyzed theoretically.[37] They found broad reflected in-plane atomic distributions, which can be interpreted in terms of a very corrugated and attractive PES. Sharp specular features are also present in the experimental distributions. These features are attributed to scattering of excited atoms [states N(^2D) and N(^2P)], which are subject to a much more repulsive PES.[38] In these experiments, a beam containing a mixture of N and N_2 was used, and it is assumed that those excited atoms are also contained in the beam. Theory input is needed to determine the fate of each species contained in the beam.

Previous theoretical work on the N adsorption dynamics showed that energy dissipation channels become relevant at low E_i^T values.[30] In fact, only less than 10% of the atoms are adsorbed at $E_i^T > 2.5\,\text{eV}$. Energy dissipation into Ag lattice vibrations is the main energy loss channel, and it is responsible for atom trapping, whereas excitation of *e-h* pairs contributes to the subsequent stabilisation of N at the equilibrium hollow adsorption sites. It has also been shown that an adiabatic model suffices to account for the angular distributions of the final kinetic energies of the reflected N atoms, albeit energy dissipation channels are required to obtain a good match with the experimental values.[8] As in N adsorption, dissipation into lattice phonons also comes through as the dominant energy loss mechanism in N reflection.

The present paper is an exhaustive study of the reflection problem. The dependence of reflec-

tion dynamics on initial conditions and energy loss channels is analysed in depth. We establish a direct connection between the topographic features of the adiabatic PES and the experimentally measured atom and energy in-plane distributions.

The paper is organised as follows: first, the *ab-initio* calculated three-dimensional PES is described and the quality of the interpolation is checked; second, the theoretical parameters of the MD simulations are detailed; then, results for a monoenergetic beam and a non-monoenergetic, or so-called effusive beam, are presented. For each type of beam the angular distributions of the reflected atoms and their energies are analysed in terms of the incident angle and the energy dissipation mechanisms involved; finally, conclusions are drawn.

Theoretical model

Potential energy surface for N/Ag(111)

The interaction energy of the N atom with the Ag(111) surface is here described with a full adiabatic 3D PES that gives the system's energy as a function of the atomic position (X,Y,Z). All *ab-initio* data are obtained with the DFT-based VASP code,[39–42] which uses a plane-wave basis set to expand the system wave functions and is particularly efficient to model metallic surfaces. The values of relevant VASP parameters are chosen so that *ab-initio* energies are calculated to a prescribed accuracy. The exchange-correlation energy is modeled within the generalized gradient approximation (GGA) and using the Perdew-Wang energy functional (PW91).[43] Possible dynamics effects brought on by the particular choice of the exchange correlation functional can be found elsewhere.[44] The electron-core interaction is described with ultra-soft pseudopotentials.[45] The energy cutoff in the plane-wave expansion is 453 eV, corresponding to a high precision VASP calculation; the fractional occupancies are determined through the broadening approach of Methfessel and Paxton[46] with $N = 1$ and $\sigma = 0.2$ eV; and the Brillouin-zone integration is performed with a $5\times5\times1$ Gamma Centered Grid of special k points.[47]

The Ag lattice constant, obtained by minimizing the energy for a bulk calculation, is $a = 4.17$

Å, which compares well with the experimental value of 4.09 Å.[48] The Ag(111) surface is modeled by means of the supercell+slab scheme. A 5-layer slab is used with a (2x2) cell in the plane parallel to the surface (N atomic coverage $\Theta = 0.25$) and a supercell of length 24.08 Å along the surface normal ($\hat{z}$ axis). The latter length guarantees no interactions between the surface and the gas N atom when the N atom is located midway between slabs. This ensures a reasonable representation of the asymptotic region. This configuration, in which the N atom has hardly any interaction with the surface, is chosen as the energy reference.

In order to get the surface equilibrium geometry, the interlayer distance is relaxed from its bulk value $d_0 = 2.408$ Å. The third layer is kept fixed during the relaxation process, which continues until the difference in energy between consecutive iterations is less than 1 meV. Even if the experimental results show a small contraction of the first interlayer distance d_{12} (-2%) and a smaller expansion of the second interlayer d_{23} ($+0.5\%$),[49,50] surface relaxations are found to be negligible in our calculations. Once relaxed, the slab is kept frozen for the calculations that follow.

Given the open-shell electronic structure of the N atom ($1s^2 2s^2 2p^3$), an adequate description of the system's ground state requires a spin polarized calculation. The system energy is calculated for 615 different positions (X_i, Y_i, Z_i) of the N atom over the frozen Ag(111) surface. The 3D grid consists of 41 equidistant points Z in the range -1.5 Å $\leq Z \leq 6.5$ Å, with $Z = 0$ corresponding to the topmost surface layer height, and 15 sites [(X,Y) values] uniformly distributed within the unit cell, as shown in Figure 1. Once the energy grid is calculated, the PES is built by interpolation of the *ab-initio* data. The Corrugation Reducing Procedure[13] is used to transform the energy grid into one for the auxiliary less corrugated function $F(X_i, Y_i, Z_i)$, $i = 1, ...615$, which is spline-interpolated over the Z coordinate. Then a Fourier expansion is used to interpolate over (X,Y) and the obtained value $F(X,Y,Z)$ is transformed back to get the energy $E(X,Y,Z)$. The Fourier method is preferred over the alternative 2D periodic spline interpolation, because it profits from the symmetry properties of the system, which are therefore preserved in the resulting PES.

In Figure 2 some quality after-checks of the interpolation are displayed. The output of the constructed 3D PES is compared to *ab-initio* off-grid values. The Z interpolation is tested both

for in-grid (top-left graph) and off-grid (top-right graph) sites. Also, for fixed $Z = 2.0$ Å, the XY interpolation is checked along the crystallographic directions $\langle \bar{1}, 0, 1 \rangle$ and $\langle 1, \bar{2}, 1 \rangle$, shown in Figure 1. We find that, for $Z > 0.7$ Å, differences with the *ab-initio* data are lower than 5 meV. We have checked that, in order to achieve similar precision, a 3D spline-interpolated PES would have required to, approximately, double the number of (X_i, Y_i) grid points. Contour plots of (X, Y) 2D-cuts are shown in Figure 3 at three Z distances from the surface. At $Z = 2.20$ Å, the PES is attractive whatever the position of N over the unit cell with an attraction slightly stronger around the top sites. At $Z = 1.20$ Å, two minima of the PES are found, located over the hollow fcc and hcp sites with energies -2.03 eV and -1.92 eV, respectively. For lower Z values ($Z = 0.85$ Å), the PES becomes repulsive over a large region of the unit cell except close to the hollow sites.

Dynamics simulation details

The dynamics of N atoms on Ag(111) is studied by means of classical trajectory calculations using a Monte Carlo sampling for the initial (X, Y) values over the unit cell. Each trajectory starts at $Z = 6.5$ Å from the surface and two incidence angles Θ_i are considered: 40° and 60° with respect to the surface normal (see Figure 4a). The incident azimuthal angle, ϕ_i, is taken along the $\langle \bar{1}, 0, 1 \rangle$ direction (see Figure 1), corresponding to the direction used in the experiments.[51] We simulate two kinds of incident beams: a monoenergetic beam with energy $E_i = 4.3$ eV and an effusive beam with an average energy $\langle E_i \rangle = 4.3$ eV that mimics the experimental conditions. The reflected particles are collected in-plane according to the procedure explained below. Knowing that few atoms are scattered in-plane ($\simeq 3$ to 5%), it is necessary to run a large number of trajectories to obtain well converged angular distributions. Therefore, 300000 trajectories are considered for the monoenergetic beam. For the effusive beam, a Metropolis algorithm is used to generate a database of initial incidence energies. In order to reproduce the energy distribution of the experimental beam, 600000 trajectories are required (see Figure 5).

We classify the trajectories according to the following exit channels: (i) reflection, when the atom is bounced back to the starting distance of 6.5 Å with a velocity vector that points towards

the vacuum; (ii) absorption, when the atom reaches the surface ($Z = 0$ Å) with a velocity vector that points towards the bulk; (iii) atomic trapping, when the atom is neither reflected nor absorbed after the maximum integration time ($t_{max} = 10$ ps). With the use of an energy criterion, we have checked in a previous work that these atoms are in fact adsorbed over the hollow sites.[30]

Two energy dissipation channels are incorporated in the calculations to take into account the energy exchange to lattice vibrations and to electronic excitations. The Generalized Langevin Oscillator (GLO) model is used to account for phonon excitations and de-excitations.[6,52] The Ag atomic mass is associated to the surface oscillators and ghost particles. The oscillation frequencies ($\omega_{x,y,z}$) are chosen equal to 5×10^{-4} a.u. (atomic units) for $\omega_{x,y}$ and 3×10^{-4} a.u. for ω_z, which correspond to the experimental vibrational frequencies for Ag(111).[53] The same values are employed for the ghost oscillators. Electron-hole (*e*-*h*) pair excitations are included using a local friction coefficient (LDFA) in the classical equations of motion.[7] This friction coefficient is calculated using DFT for an atom embedded in a free electron gas.[54]

In the experiments, the scattered particles are detected in-plane (i.e. along the $\langle \bar{1}, 0, 1 \rangle$ direction) and per solid angle. Therefore, an adapted procedure should be considered in order to account for our results per solid angle. We propose to use a virtual detector representing the experimental detector, localized by the vector position $\overrightarrow{r_d}$ (see Fig .Figure 4b). This detector is able to rotate in the (X,Z) plane in order to detect scattered particles at any outgoing polar angle Θ_f. We also define $\overrightarrow{r_a}$ as the vector position of the reflected atoms. The procedure relies on the comparison of an acceptance angle τ_{ref} that defines the circular aperture of the detector with the angle τ defined as the angle between the virtual detector and the reflected atoms [$\tau = (\overrightarrow{r_d}, \overrightarrow{r_a})$]. After simplifications, τ can be written as:

$$\tau = \arccos\left(\sin\Theta_d \sin\Theta_a \cos\phi_a + \cos\Theta_d \cos\Theta_a\right) \tag{1}$$

where the subscripts d and a refer to the detector and the reflected atom, respectively. Θ and ϕ are polar and azimuthal final angles, respectively. The ϕ_d angle equal to 0° corresponds to the $\langle \bar{1}, 0, 1 \rangle$ direction. Our criterion of selection is that the atoms that fulfill the condition $\tau \leq \tau_{ref}$ are detected.

This simple procedure is used to evaluate in an accurate way the angular distributions that will

be later compared with the experimental ones. The results obtained are not much sensitive to the τ_{ref} value when this angle is lower than 5°. Nevertheless, in order to obtain reasonable statistics, it is required to use a not too low τ_{ref} value. The results given below have been obtained for $\tau_{ref} = 4°$.

Results

Scattering results for a monoenergetic beam

As mentioned above, two energy dissipation channels are included in the classical trajectory calculations: *e-h* pairs and phonon excitations. In the following, three kinds of dynamics simulations are considered in order to deal with the effects of the dissipation channels on the angular distribution and energy loss of the scattered N atoms: (i) using an adiabatic and frozen surface model (i.e. neglecting any dissipation channels), (ii) using the GLO model and (iii) using the LDFA+GLO model that includes both dissipation channels. Further details about this combination are given elsewhere.[8,30]

In order to assess the effect of the effusive beam on the experimental results,[36] we start by using a monoenergetic beam of $E_i = 4.3$ eV. This simulation shows that reflection is the dominant process. The reflection probability is 1 within the adiabatic model and close to 1 after inclusion of phonons (less than 1% of N atoms are adsorbed and none of them are absorbed).[30]

Angular distribution

The angular distributions of a monoenergetic beam of N atoms scattered off Ag(111) are shown in Figure 6. In agreement with the experimental results, N scattering yields a broad angular distribution no matter the values of the initial conditions, such as the incidence angle, Θ_i, or the surface temperature, T_S. These results reflect the PES topology, which shows attractive wells above the hollow sites, as well as strong corrugation in (X,Y) close to the surface (see Figure 2 and Figure 3). The influence of the dissipation channels on the angular distributions is negligible and confirms

conclusions extracted previously, namely that important aspects of the scattering dynamics are already captured by the adiabatic calculations.[8] In the experimental studies,[36] the authors propose to decompose the angular distribution in two components: a broad component attributed to scattering of the ground state N(^4S) atoms, and a sharp peak that may be attributed to excited states of N(^2D,^2P) atoms also present in the experimental beam. Our results are consistent with this proposal as our ground state dynamics simulation correctly reproduces the broad component but fails to produce the sharp specular peak.

The only differences obtained between our theoretical results and the experimental ones are the peaks present in our calculations that are unrelated to the excited states effect. At $\Theta_i = 40^\circ$, the angular distributions exhibit a peak close to the specular direction, and at $\Theta_i = 60^\circ$ the distributions present a peak at small Θ_f. An additional study, using various incidence angles Θ_i ranging from 0° to 80°, allows us to unravel the general aspects of the angular distributions. From 0° to 40°, a specular peak is obtained that becomes more important for small Θ_i values. At $\Theta_i = 40^\circ$, this peak corresponds to a slightly sub-specular reflection. This reflection without memory loss of the initial conditions of N atoms is important for low incident angles but dissapears for higher angles ($\Theta_i > 40^\circ$) leading to an homogeneous broad distribution. This can be understood in terms of the initial perpendicular energy $E_i^\perp$ ($E_i^\perp = E_i^T \cos^2\Theta_i \approx 2.5$ eV at $\Theta_i = 40^\circ$), that reduces the effect of the attractive wells for low Θ_i and makes N atoms more sensitive to them for high Θ_i. Note that the peak obtained at $\Theta_i = 60^\circ$ for smaller outgoing angles is not observed for other incidence angles.

A detailed analysis of the trajectories can be done by performing a decomposition of the angular distribution as shown in Figure 7 for $\Theta_i = 60^\circ$. This decomposition is based on the minimum distance to the surface Z_{ref} reached by the N atoms. By using this criterion, three main groups of trajectories can be distinguished:

(i) Group 1: reflection at large distances ($Z_{ref} > 1.45$ Å), which occurs over top sites. There, the PES at top sites is repulsive from $Z \leq 1.75$Å due to the presence of Ag atoms (see Figure 3). Thus, reflection happens far away from the surface, where the corrugation is less important. That allows the N atoms to keep some memory of their initial conditions, leading to scattering

close to the specular direction. The broadness of the angular distribution is due to the fact that atoms reflected at the downhill potential are scattered at large Θ_f ($\gtrsim 65^\circ$) whereas the atoms reflected at the uphill potential are scattered at small Θ_f ($\lesssim 65^\circ$), as already shown before in the scattering of noble gas atoms.[55,56]

(ii) Group 2: reflection at intermediates distances ($0.85 < Z_{ref} \leq 1.45$ Å), characterized by a broad distribution. Reflection happens on a large region of the unit cell basically located on channels along the $\langle \bar{1}, 0, 1 \rangle$ direction (see Figure 1). For a non negligible number of atoms, the reflection process is strongly influenced by the hollow wells leading to scattering with small Θ_f ($\Theta_f < 40^\circ$), as it happens for group 3 (see below). Other N atoms are reflected in a relatively flat PES region along the line $Y = 0.5$ (see Figure 3) that roughly yields a reflection around the specular direction. Dynamics of N atoms is quite complex for this group of trajectories. For instance, the number of lateral rebounds (a lateral rebound corresponds to a change in the sign of the Y component of the momentum) is large due to collisions in the repulsive part of the PES close to the top sites. These collisions allow focusing of the N atoms in channels along the $\langle \bar{1}, 0, 1 \rangle$ direction prior to reflection. Note that the consideration of groups 1 and 2 only gives a very good agreement with experimental data.

(iii) Group 3: reflection close to the surface ($Z_{ref} \leq 0.85$ Å). This group of trajectories is clearly responsible for the peak obtained at small angles. It is worth to note that this peak is observed for very specific initial conditions. Indeed, as we will show below, it disappears for other initial kinetic energies E_i^T and seems to be present only for a narrow energy range around 4.3 eV. Moreover, upon consideration of all scattered particles (in-plane and out-of-plane), this feature would be lost from the total signal. This kind of reflection is strongly influenced by the adsorption wells that accelerate the N atoms towards the surface and focus them in a restricted area of the PES. Due to the presence of Ag atoms, the reflected atoms are focused into one particular direction over the surface, specially into the direction connecting the two hollow sites (hcp $\rightarrow$ fcc or fcc $\rightarrow$ hcp). This direction corresponds to the most favorable

path back into the gas phase (except for backscattering directions not visible by the detector). This favored direction involves an overall deviation from the initial angle $\phi_i = 0°$. The final average value is $\langle \phi_f \rangle = 32°$ for this group of trajectories, whereas it is $\langle \phi_f \rangle = 14°$ for all the detected trajectories. This means that, for the in-plane detection conditions considered here (see Figure 4), these atoms can only be detected for small Θ_f values.

It should be noted that this decomposition is arbitrarily defined, as there are no clear crossovers for Z_{ref} values, and it is used here only for explanatory purposes.

Energy dissipation

We now focus on the energy dissipation of N atoms through phonons and *e-h* pair excitations. As in the experimental studies,[36] we show in Figure 8 the ratio between the average final energy and the initial energy $\left(\frac{\langle E_f^T \rangle}{E_i^T}\right)$ as a function of the total scattering angles Θ_t (see Figure 4a). The bracket notation is here omitted for E_i^T as the initial beam is monoenergetic.

For all the initial conditions (Θ_i,T_S) considered in this work, our results follow the experimental trend, i.e. the average final energy $\langle E_f^T \rangle$ of N atoms increases with decreasing Θ_t (increasing Θ_f). These theoretical results (in particular those obtained with the GLO model) are very close to the hard-sphere model, suggesting a single binary collision with the surface.[56,57] An analysis of the number of rebounds confirms these results (a rebound is defined as a sign change from negative to positive in the perpendicular component of the atomic velocity). Indeed, the average number of rebounds $\langle N_r \rangle$ at $\Theta_i = 60°$ and $T_S = 500$ K for all the detected atoms, independently of outgoing angles, is only 1.4. In other words, most N atoms make a single rebound on the surface before being reflected. This is the manifestation of a very direct reflection process.

The difference between the results obtained with GLO and LDFA+GLO shows that the *e-h* pair excitations have a negligible influence on the energy loss, no matter the initial conditions. Therefore, the phonon excitations are responsible for the energy transfer observed experimentally. Despite the good agreement of the simulation results with the experimental ones for large scattering angles, the large increase of the energy ratios $\left(\frac{\langle E_f^T \rangle}{\langle E_i^T \rangle} > 1\right)$ for smaller Θ_t is not reproduced. As

explained elsewhere,[8] this unlikely behavior is due to the broad energy distribution of the beam used in the experiments (see Figure 5). The next section is devoted to the scattering of an effusive beam of N atoms and will include the explanation for this anomalous behaviour.

Scattering results for an effusive beam

As the *e-h* pair excitations have a negligible effect on the scattering of N off Ag(111), the following study will not consider this dissipation channel. In the case of the simulation of an effusive beam (Figure 5), the reflection process still dominates. However, the adsorption process becomes non negligible since $\sim 10\%$ of the N atoms are now adsorbed on the surface when phonon excitations are included. This is due to low energy atoms present in the effusive beam (mainly $E_i^T \leq 2$ eV) that are adsorbed at the hollow sites (fcc and hcp, see Figure 1), as shown in Ref.[30] Moreover, as the effusive beam includes very high energies, the simulation results exhibit a non-zero absorption probability. The absorption process occurs at the vicinity of the hollow sites for N atoms with $E_i^T > 9$ eV. However, this process is negligible since it represents less than 0.1% of the events.

Angular distribution

Angular distributions obtained with an effusive beam ($\langle E_i^T \rangle = 4.29$ eV) are shown in Figure 9. Similarly to the monoenergetic beam, the adiabatic calculations incorporate the main information on the scattering dynamics, since the dissipation channel affects only slightly to the angular distributions. Compared to the results obtained for a monoenergetic beam, the angular distributions are broader with these new initial conditions and closer to the experimental data. The main difference with the experimental broad component appears at low outgoing angles for the two considered incidence angles. These differences are related to the peak at low angles described previously. Nevertheless, the differences are largely attenuated when the effusive beam is considered. In particular, the peak observed for the monoenergetic beam at $\Theta_i = 60^\circ$ for small outgoing angles Θ_f is strongly reduced. This confirms the sensitivity of this peak to the initial conditions and PES topography. In addition, calculations with an effusive beam still do not account for the sharp peak

observed experimentally at $\Theta_i = 60^\circ$ confirming the assumption about the role of N first excited states.

The effect of the initial kinetic energy E_i^T on the angular distribution is shown in Figure 10 for $\Theta_i = 60^\circ$ with both the adiabatic and GLO models. According to this figure, a large variety of angular distributions can be obtained by changing E_i^T. At lower E_i^T ($E_i^T = 1.0$ eV), the angular distribution is a cosine-like distribution characteristic of a memory loss of the initial conditions. This is due to the attraction effect of the wells, that is enhanced for smaller initial energy ($E_i^\perp \approx 0.3$ eV for $E_i^T = 1.0$ eV). Indeed, the N atoms are accelerated considerably by the wells towards the surface and reach PES regions that appear strongly corrugated compared to the small available energy of N atoms, leading to a memory loss of the initial conditions. At higher E_i^T ($E_i^T \gtrsim 6.0$ eV), a specular distribution appears that becomes very significant at 10.0 eV. Due to the high $E_i^\perp$, the attraction effect of the wells is reduced. As a consequence, N atoms are little affected by the surface corrugation, allowing preservation of the memory of the initial conditions. From Figure 10, the attenuation of the peak at small Θ_f obtained with an effusive beam is explained since no angular distribution (except the one for $E_i^T = 4.3$ eV) exhibits such a peak for all the E_i^T considered. Nevertheless, this structure does not totally disappear in Figure 9, since the initial energy range around 4 eV represents highly probable events according to the experimental beam distribution (Figure 5).

This kind of decomposition of the effusive beam according to the initial energy range of N atoms had already been performed in previous works for the experimental scattering of F atoms on a fluorinated Si surface where two distinct scattering processes had also been suggested:[58,59] (i) multiple bounce/indirect scattering giving a cosine distribution that corresponds to our lower E_i^T and (ii) single bounce/direct scattering resulting in a broad specular distribution that corresponds to our higher E_i^T. However, note that, in our case, we can not discriminate between the two scattering processes by using the number of rebounds, since it remains quite low at any E_i^T. For instance, we find that $N_r = 1.7$ for $\langle E_i^T \rangle < 1.0$ eV and $N_r = 1.4$ for $\langle E_i^T \rangle > 6.0$ eV. This small difference is due to the fact that, at low initial energies, atoms suffering a larger number of rebounds (> 2)

are adsorbed. As explained above, the two scattering processes are caused by the capability of the adsorption wells to influence or not the trajectory.

The comparison of the adiabatic and GLO calculations in Figure 10 shows that the E_i^T-dependence of the angular distribution is a pure dynamic effect not related to any energy dissipation. Similar conclusions could be drawn for $\Theta_i = 40^\circ$ though the specular distribution observed for higher E_i^T atoms at $\Theta_i = 60^\circ$ is only present in a more restrictive intermediate energy range for $\Theta_i = 40^\circ$. Note that for a given E_i^T, the perpendicular energy for $\Theta_i = 40^\circ$ doubles the one corresponding to $\Theta_i = 60^\circ$. This induces a much deeper penetration of the atoms into the surface, leading to a new scattering picture defined by the interactions at a height closer to 0 Å in the neighborhood of the top sites. As an example, at $E_i^T = 10.0$ eV and $\Theta_i = 40^\circ$ the angular distribution does not exhibit a specular peak but a supra-specular peak (peak at $\Theta_f \simeq 50^\circ$) that is even more pronounced for higher E_i^T and shifted to $\simeq 65^\circ$. This new scattering picture is also observed for $\Theta_i = 60^\circ$ at much higher E_i^T.

Energy dissipation

The energy distributions of the scattered atoms obtained with the effusive beam are presented in Figure 11. In contrast to the monoenergetic calculations, a strong increase at smaller Θ_t angles is observed with energy ratios greater than one. This increase is observed for all initial conditions, but it is more pronounced at $\Theta_i = 60^\circ$. The angular distributions at various kinetic energies E_i^T, shown in Figure 10, allow us to explain this behavior. At small outgoing angles Θ_f (i.e. large Θ_t), the scattered N atoms are mostly low energy atoms ($E_i^T \leq 2.0$ eV) together with atoms of $E_i^T \simeq 4.0$ eV that follow the group 3 trajectories described above. As a result, the average initial energy $\langle E_i^T \rangle$ of the atoms scattered at high Θ_t ($\Theta_t > 100^\circ$) is slightly lower than $\langle E_i^T \rangle = 4.29$ eV, leading to low values of the energy ratio even without the inclusion of phonon excitations ($\frac{\langle E_f^T \rangle}{\langle E_i^T \rangle} < 1$ for the adiabatic model). When the outgoing angles Θ_f increase and get closer to the specular direction, the relative number of high energy reflected atoms increases as well. In that case, the average final energy increase makes it possible to get a final-to-initial average energy ratio greater than one. The

fact that the adiabatic simulation already reproduces this behavior proves that it is a trajectory effect not related to any energy dissipation channel (see Figure 10). This emphasizes the importance of an accurate PES determination to deal with the N scattering off Ag(111). It is worth noting that for $\Theta_i = 40^\circ$ the evolution of the final-to-initial energy ratio with Θ_t is non-monotonic. This is due to the more complex dependence of the angular distributions with E_i^T, as underlined in the previous section.

The quantitative agreement with the experimental results is improved when phonon excitations are included. Yet, the largest difference with the experimental results is observed around the specular direction. This is consistent with the presence in the experimental beam of excited N atoms that are specularly reflected and that are not accounted for in the simulation.[36]

Conclusions

The objective of the current work was to study theoretically the non-reactive scattering of N atoms off Ag(111) surfaces in comparison with recent experimental results. This theoretical work is based on the development of an accurate multidimensional potential energy surface combined with the use of an elaborated model to simulate energy dissipation channels (phonons and electron-hole pairs excitations).

A monoenergetic beam as well as an effusive beam have been considered in this work. For both cases, the results of the dynamics calculations show broad angular distributions in qualitative agreement with the experimental results. The effect of dissipation channels on the angular distributions is negligible. The detailed study of the reflection process for a monoenergetic beam reveals very different dynamics depending on the impact position of the atoms in the unit cell. Thus, scattering dynamics is either ruled by the attractive hollow wells, leading to reflection at small outgoing angles, or by the repulsive top sites, leading to reflection around the specular direction. The energy loss results are also in good agreement with experimental information and follow the simple model of binary collisions. This is linked to a direct reflection process with few rebounds of N atoms.

Theory-experiment agreement is however not as good at small scattering angles and requires the use of an effusive beam to explain the strong increase of the average final energy. Electron-hole pair excitations are shown to have a negligible influence on the energy loss. The effusive beam simulation, coupled to phonon excitations, accounts for the experimental results. We show that the increase in the final average energy of the reflected N atoms at small scattering angles is due to dynamic effects, that render different angular distributions depending on the initial energy of N atoms. In particular we observe that high energy atoms are mostly reflected at grazing outgoing angles.

Discrepancies between our results and the experimental ones are little and mostly observed at specular scattering. As suggested by Ueta et al.,[36] the results obtained for this particular direction could be due to the electronically excited N atoms present in the composition of the experimental beam. Further work would be then necessary to study the exact role played by the electronically excited states of N atoms.

Acknowledgement

We acknowledge fruitful discussions with H.F. Busnengo and A.W. Kleyn regarding the PES and dynamical calculations. This work has been supported in part by the Basque Departamento de Educación, Universidades e Investigación, the University of the Basque Country UPV/EHU (Grant No. IT-366-07) and the Spanish Ministerio de Ciencia e Innovación (Grant No. FIS2010-19609-C02-02). M.B.-R. acknowledges financial support from the Gipuzkoako Foru Aldundia and the European Union 7th Framework Programme (FP7/2007-2013) under grant agreement no. FP7-PEOPLE-2010-RG276921. Computational resources were provided by the DIPC computing center.

References

(1) Díez Muiño, R., Busnengo, H. F., Eds. *Dynamics of Gas-Surface Interactions: Atomic-level Understanding of Scattering Processes at Surfaces*; Springer Series in Surface Sciences;

Springer, 2013; Vol. 50.

(2) Groß, A. Reactions at Surfaces Studied by Ab Initio Dynamics Calculations. *Surf. Sci. Rep.* **1998**, *32*, 291–340.

(3) Kroes, G.-J.; Groß, A.; Baerends, E.-J.; Scheffler, M.; McCormack, D. A. Quantum Theory of Dissociative Chemisorption on Metal Surfaces. *Acc. Chem. Res.* **2002**, *35*, 193–200.

(4) Kroes, G. J. Towards Chemically Accurate Simulation of Molecule–Surface Reactions. *Phys. Chem. Chem. Phys.* **2012**, *14*, 14966–14981.

(5) Gravielle, M. S.; Bocan, G. A.; Díez Muiño, R. Diffraction of Swift Atoms after Grazing Scattering from Metal Surfaces: N/Ag(111) System. *Phys. Rev. A* **2010**, *82*, 052904.

(6) Busnengo, H. F.; Dong, W.; Salin, A. Trapping, Molecular Adsorption, and Precursors for Nonactivated Chemisorption. *Phys. Rev. Lett.* **2004**, *93*, 236103.

(7) Juaristi, J. I.; Alducin, M.; Díez Muiño, R.; Busnengo, H. F.; Salin, A. Role of Electron-Hole Pair Excitations in the Dissociative Adsorption of Diatomic Molecules on Metal Surfaces. *Phys. Rev. Lett.* **2008**, *100*, 116102.

(8) Martin-Gondre, L.; Alducin, M.; Bocan, G. A.; Díez Muiño, R.; Juaristi, J. I. Competition between Electron and Phonon Excitations in the Scattering of Nitrogen Atoms and Molecules off Tungsten and Silver Metal Surfaces. *Phys. Rev. Lett.* **2012**, *108*, 096101.

(9) Fuchsel, G.; Klamroth, T.; Monturet, S.; Saalfrank, P. Dissipative Dynamics within the Electronic Friction Approach: the Femtosecond Laser Desorption of H_2/D_2 from Ru(0001). *Phys. Chem. Chem. Phys.* **2011**, *13*, 8659–8670.

(10) Meyer, J.; Reuter, K. Electron–Hole Pairs during the Adsorption Dynamics of O_2 on Pd(100): Exciting or Not? *New J. Phys.* **2011**, *13*, 085010.

(11) Muzas, A. S.; Juaristi, J. I.; Alducin, M.; Díez Muiño, R.; Kroes, G. J.; Díaz, C. Vibrational Deexcitation and Rotational Excitation of H_2 and D_2 Scattered from Cu(111): Adiabatic versus Non-Adiabatic Dynamics. *J. Chem. Phys.* **2012**, *137*, 064707.

(12) Nattino, F.; Díaz, C.; Jackson, K. A.; Kroes, G. J. Effect of Surface Motion on the Rotational Quadrupole Alignment Parameter of D_2 Reacting on Cu(111). *Phys. Rev. Lett.* **2012**, *108*, 236104.

(13) Busnengo, H. F.; Salin, A.; Dong, W. Representation of the 6D Potential Energy Surface for a Diatomic Molecule Near a Solid Surface. *J. Chem. Phys.* **2000**, *112*, 7641–7651.

(14) Hou, H.; Huang, Y.; Gulding, S. J.; Rettner, C. T.; Auerbach, D. J.; Wodtke, A. M. Enhanced Reactivity of Highly Vibrationally Excited Molecules on Metal Surfaces. *Science* **1999**, *284*, 1647–1650.

(15) Smith, R. R.; Killelea, D. R.; DelSesto, D. F.; Utz, A. L. Preference for Vibrational over Translational Energy in a Gas-Surface Reaction. *Science* **2004**, *304*, 992–995.

(16) Díaz, C.; Olsen, R. A. A Note on the Vibrational Efficacy in Molecule-Surface Reactions. *J. Chem. Phys.* **2009**, *130*, 094706.

(17) Rettner, C.; Stein, H.; Schweizer, E. K. Effect of Collision Energy and Incidence Angle on the Precursor-Mediated Dissociative Chemisorption of N_2 on W(100). *J. Chem. Phys.* **1988**, *89*, 3337–3341.

(18) Rettner, C.; Schweizer, E. K.; Stein, H. Dynamics of the Chemisorption of N_2 on W(100): Precursor-Mediated and Activated Dissociation. *J. Chem. Phys.* **1990**, *93*, 1442–1454.

(19) Romm, L.; Katz, G.; Kosloff, R.; Asscher, M. Dissociative Chemisorption of N_2 on Ru(001) Enhanced by Vibrational and Kinetic Energy: Molecular Beam Experiments and Quantum Mechanical Calculations. *J. Phys. Chem. B* **1997**, *101*, 2213–2217.

(20) Diekhöner, L.; Mortensen, H.; Baurichter, A.; Jensen, E.; Petrunin, V. V.; Luntz, A. C. N_2 Dissociative Adsorption on Ru(0001): The Role of Energy Loss. *J. Chem. Phys.* **2001**, *115*, 9028–9035.

(21) Díaz, C.; Vincent, J. K.; Krishnamohan, G. P.; Olsen, R. A.; Kroes, G. J.; Honkala, K.; Norskov, J. Multidimensional Effects on Dissociation of N_2 on Ru(0001). *Phys. Rev. Lett.* **2006**, *96*, 096102.

(22) Alducin, M.; Díez Muiño, R.; Busnengo, H. F.; Salin, A. Why N_2 Molecules with Thermal Energy Abundantly Dissociate on W(100) and Not on W(110). *Phys. Rev. Lett.* **2006**, *97*, 056102.

(23) Alducin, M.; Díez Muiño, R.; Busnengo, H. F.; Salin, A. Low Sticking Probability in the Nonactivated Dissociation of N_2 Molecules on W(110). *J. Chem. Phys.* **2006**, *125*, 144705.

(24) Goikoetxea, I.; Juaristi, J. I.; Alducin, M.; Díez Muiño, R. Dissipative Effects in the Dynamics of N_2 on Tungsten Surfaces. *J. Phys.: Condens. Matter* **2009**, *21*, 264007.

(25) Goikoetxea, I.; Alducin, M.; Díez Muiño, R.; Juaristi, J. I. Dissociative and Non-Dissociative Adsorption Dynamics of N_2 on Fe(110). *Phys. Chem. Chem. Phys.* **2012**, *14*, 7471–7480.

(26) Martin-Gondre, L.; Crespos, C.; Larrégaray, P.; Rayez, J. C.; van Ootegem, B.; Conte, D. Is the LEPS Potential Accurate Enough to Investigate the Dissociation of Diatomic Molecules on Surfaces? *Chem. Phys. Lett.* **2009**, *471*, 136–142.

(27) Martin-Gondre, L.; Crespos, C.; Larrégaray, P.; Rayez, J. C.; van Ootegem, B.; Conte, D. Dynamics Simulation of N_2 Scattering onto W(100,110) Surfaces: A Stringent Test for the Recently Developed Flexible Periodic London–Eyring–Polanyi–Sato Potential Energy Surface. *J. Chem. Phys.* **2010**, *132*, 204501.

(28) Raukema, A.; Dirksen, R. J.; Kleyn, A. W. Probing the (Dual) Repulsive Wall in the Interaction of O_2 , N_2 , and Ar with the Ag(111) Surface. *J. Chem. Phys.* **1995**, *103*, 6217–6231.

(29) Ueta, H.; Gleeson, M. A.; Kleyn, A. W. The Interaction of Hyperthermal Nitrogen with N-Covered Ag(111). *J. Chem. Phys.* **2011**, *135*, 074702.

(30) Martin-Gondre, L.; Bocan, G. A.; Alducin, M.; Juaristi, J. I.; Díez Muiño, R. Energy Dissipation Channels in the Adsorption of N on Ag(111). *Comp. Theo. Chem.* **2012**, *990*, 126–131.

(31) Carter, R. N.; Murphy, M. J.; Hodgson, A. On the Recombinative Desorption of N_2 from Ag(111). *Surf. Sci.* **1997**, *387*, 102–111.

(32) Soon, A.; Wong, A.; Lee, M.; Todorova, M.; Delley, B.; Stampfl, C. Nitrogen Adsorption and Thin Surface Nitrides on Cu(111) from First-Principles. *Surf. Sci.* **2007**, *601*, 4775–4785.

(33) Lykke, K.; Kay, B. D. State-To-State Inelastic and Reactive Molecular Beam Scattering from Surfaces. *SPIE Proc.* **1990**, *1208*, 18.

(34) Rettner, C. Reaction of an H-Atom Beam with Cl/Au(111): Dynamics of Concurrent Eley–Rideal and Langmuir–Hinshelwood Mechanisms. *J. Chem. Phys.* **1994**, *101*, 1529–1546.

(35) Rettner, C.; Auerbach, D. J. Dynamics of the Eley-Rideal Reaction of D Atoms with H Atoms Adsorbed on Cu(111): Vibrational and Rotational State Distributions of the HD Product. *Phys. Rev. Lett.* **1995**, *74*, 4551–4554.

(36) Ueta, H.; Gleeson, M. A.; Kleyn, A. W. Scattering of Hyperthermal Nitrogen Atoms from the Ag(111) Surface. *J. Phys. Chem. A* **2009**, *113*, 15092–15099.

(37) Blanco-Rey, M.; Martin-Gondre, L.; Díez Muiño, R.; Alducin, M.; Juaristi, J. I. Dynamics of Nitrogen Scattering off N-Covered Ag(111). *J. Phys. Chem. C* **2012**, *116*, 21903–21912.

(38) Kokh, D. B.; Buenker, R. J.; White, J. L. Trends in Adsorption of Open-Shell Atoms and Small Molecular Fragments on the Ag(111) Surface. *Surf. Sci.* **2006**, *600*, 5104–5113.

(39) Kresse, G.; Hafner, J. Ab initio Molecular Dynamics for Liquid Metals. *Phys. Rev. B* **1993**, *47*, 558–561.

(40) Kresse, G.; Hafner, J. Ab initio Molecular Dynamics for Open-Shell Transition Metals. *Phys. Rev. B* **1993**, *48*, 13115–13118.

(41) Kresse, G.; Furthmüller, J. Efficiency of Ab-Initio Total Energy Calculations for Metals and Semiconductors Using a Plane-Wave basis Set. *Comput. Mater. Sci.* **1996**, *6*, 15–50.

(42) Kresse, G.; Furthmüller, J. Efficient Iterative Schemes for Ab Initio Total-Energy Calculations Using a Plane-Wave Basis Set. *Phys. Rev. B* **1996**, *54*, 11169–11186.

(43) Perdew, J. P.; Chevary, J. A.; Vosko, S. H.; Jackson, K. A.; Pederson, M. R.; Singh, D. J.; Fiolhais, C. Atoms, Molecules, Solids, and Surfaces: Applications of the Generalized Gradient Approximation for Exchange and Correlation. *Phys. Rev. B* **1992**, *46*, 6671–6687.

(44) Bocan, G. A.; Díez Muiño, R.; Alducin, M.; Busnengo, H. F.; Salin, A. The Role of Exchange-Correlation Functionals in the Potential Energy Surface and Dynamics of N_2 Dissociation on W Surfaces. *J. Chem. Phys.* **2008**, *128*, 154704.

(45) Vanderbilt, D. Soft Self-Consistent Pseudopotentials in a Generalized Eigenvalue Formalism. *Phys. Rev. B* **1990**, *41*, 7892–7895.

(46) Methfessel, M.; Paxton, A. T. High-Precision Sampling for Brillouin-Zone Integration in Metals. *Phys. Rev. B* **1989**, *40*, 3616–3621.

(47) Monkhorst, H.; Pack, J. Special Points for Brillouin-Zone Integrations. *Phys. Rev. B* **1976**, *13*, 5188–5192.

(48) Bassett, W.; Liu, L. Compression of Ag and Phase Transformation of NaCI. *J. Appl. Phys.* **1973**, *44*, 1475–1479.

(49) Lewis, L. J. Thermal Relaxation of Ag(111). *Phys. Rev. B* **1994**, *50*, 17693–17696.

(50) Statiris, P.; Lu, H.; Gustafsson, T. Temperature Dependent Sign Reversal of the Surface Contraction of Ag(111). *Phys. Rev. Lett.* **1994**, *72*, 3574–3577.

(51) Ueta, H.; Kleyn, A. W. Private communication.

(52) Tully, J. C. Dynamics of Gas–Surface Interactions: 3D Generalized Langevin Model Applied to FCC and BCC Surfaces. *J. Chem. Phys.* **1980**, *73*, 1975–1985.

(53) Ponjée, M. W. G.; Flipse, C. F. J.; Denier van der Gon, A. W.; Brongersma, H. H. Experimental Observation of Vibrational Modes on Ag(111) Along $\overline{\Gamma M}$ and $\overline{\Gamma K}$. *Phys. Rev. B* **2003**, *67*, 174301.

(54) Echenique, P.; Nieminen, R.; Ritchie, R. Density Functional Calculation of Stopping Power of an Electron Gas for Slow Ions. *Solid State Commun.* **1981**, *37*, 779–781.

(55) Rettner, C.; Barker, J.; Bethune, D. Angular and Velocity Distributions Characteristic of the Transition Between the Thermal and Structure Regimes of Gas-Surface Scattering. *Phys. Rev. Lett.* **1991**, *67*, 2183–2186.

(56) Lahaye, R. J. E. W.; Kleyn, A. W.; Stolte, S.; Holloway, S. The Scattering of Ar from Ag(111): a Molecular Dynamics Study. *Surf. Sci.* **1995**, *338*, 169–182.

(57) Niehus, H.; Heiland, W.; Taglauer, E. Low-Energy Ion Scattering at Surfaces . *Surf. Sci. Rep.* **1993**, *17*, 213–303.

(58) Hwang, G.; Anderson, C.; Gordon, M.; Moore, T.; Minton, T.; Giapis, K. Gas-Surface Dynamics and Profile Evolution During Etching of Silicon. *Phys. Rev. Lett.* **1996**, *77*, 3049–3052.

(59) Minton, T.; Giapis, K.; Moore, T. Inelastic Scattering Dynamics of Hyperthermal Fluorine Atoms on a Fluorinated Silicon Surface. *J. Phys. Chem. A* **1997**, *101*, 6549–6555.

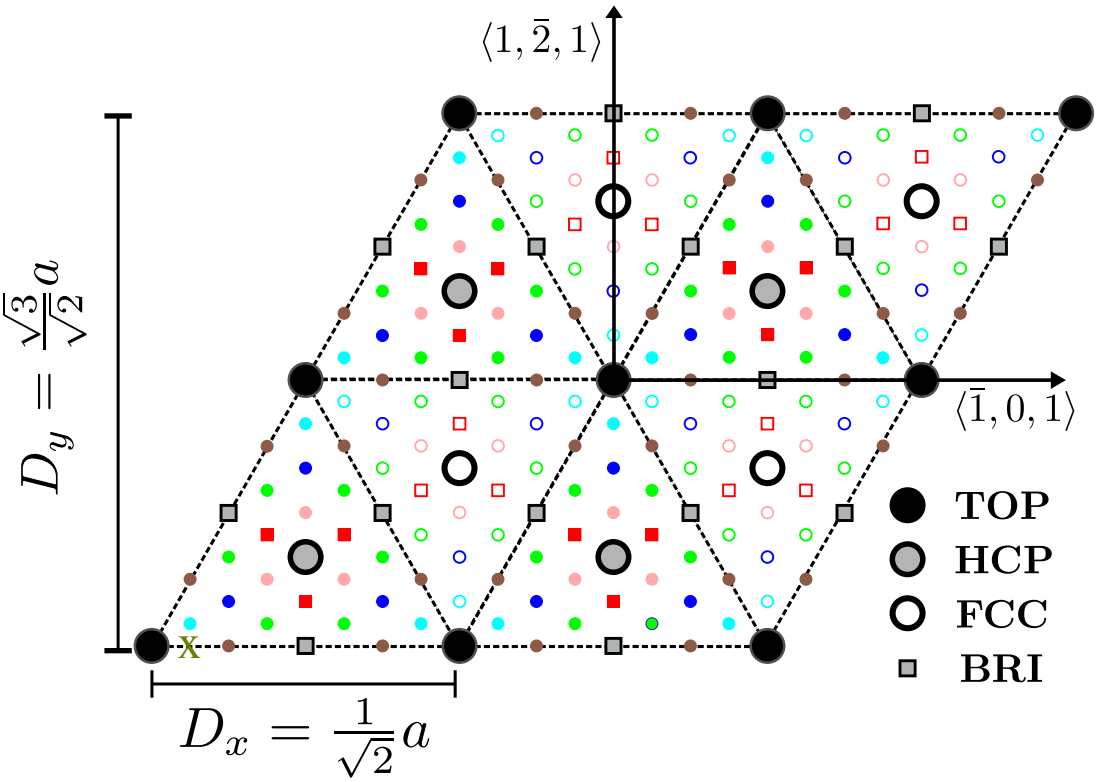

Figure 1: Surface geometry and symmetry. Symbols indicate the XY-grid, with top, hcp and fcc points placed on top of Ag atoms of the first, second and third layer, respectively. Also, directions $\langle \bar{1}, 0, 1 \rangle$ and $\langle 1, \bar{2}, 1 \rangle$ are illustrated, together with the quantities D_x, D_y and site χ, with the coordinates ($X = D_x/8$, $Y = 0$), and marked with an X. These data are referred to in Figure 2.

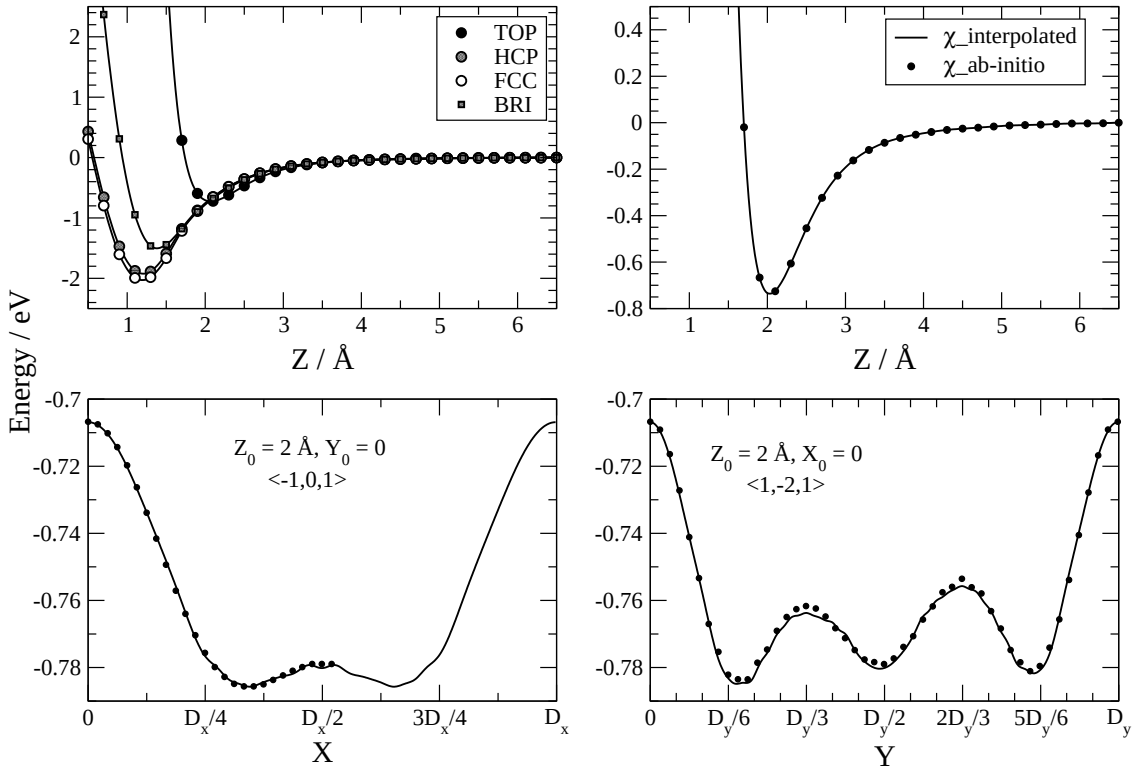

Figure 2: Top panels: Z-interpolation checks for in-grid (left) and off-grid (right) sites. Site χ is defined in Figure 1. Bottom panels: XY-interpolation checks along the stated directions, shown in Figure 1. In each graph, symbols stand for *ab-initio* data while solid lines represent interpolated results.

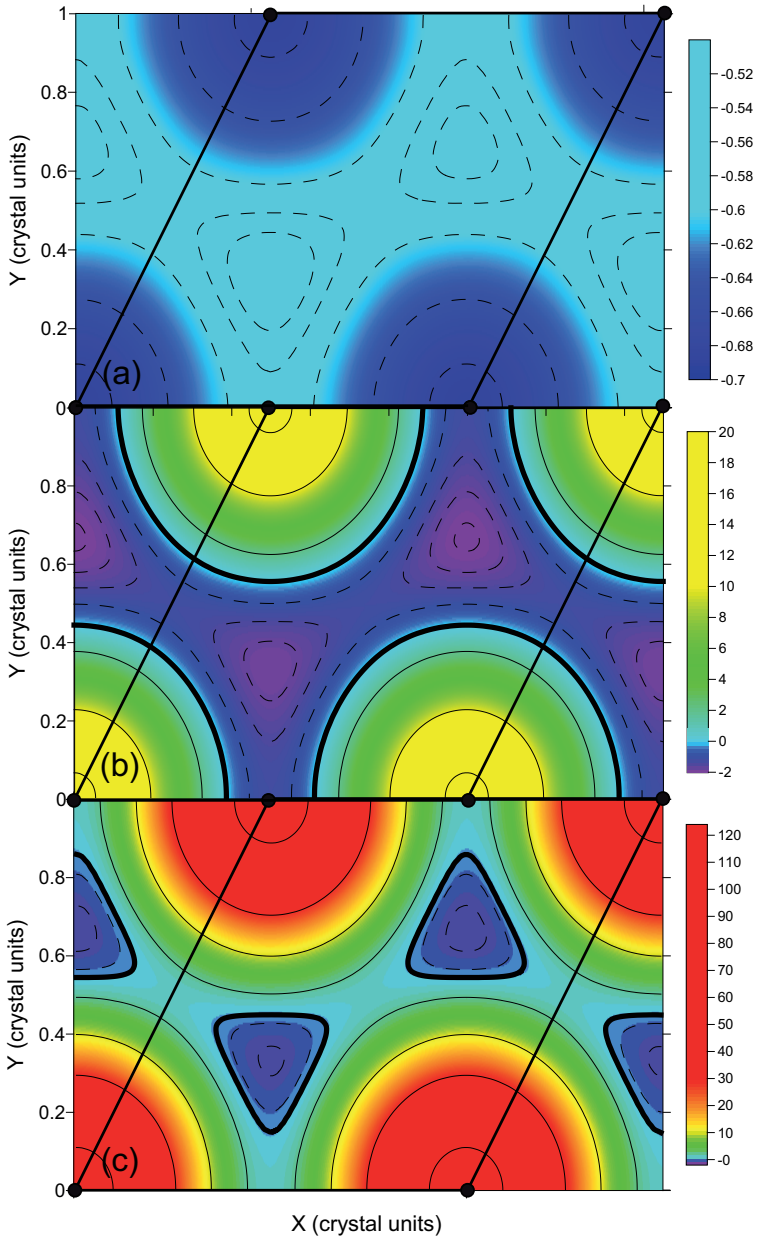

Figure 3: Contour plots of (X,Y) 2D-cuts of the N/Ag(111) PES at fixed Z distances: 2.20 Å (a), 1.20 Å (b) and 0.85 Å (c). X and Y coordinates are given in units of D_x and $D_y/2$ respectively (see Figure 1). The black thick solid line corresponds to zero potential energies. Thin solid (dashed) contour lines correspond to positive (negative) values of potential energy (eV). The contour lines are not uniformly separated and are only plotted to guide the eye. The unit cell is represented by straight black lines and the small black circles represent the Ag atoms of the first layer.

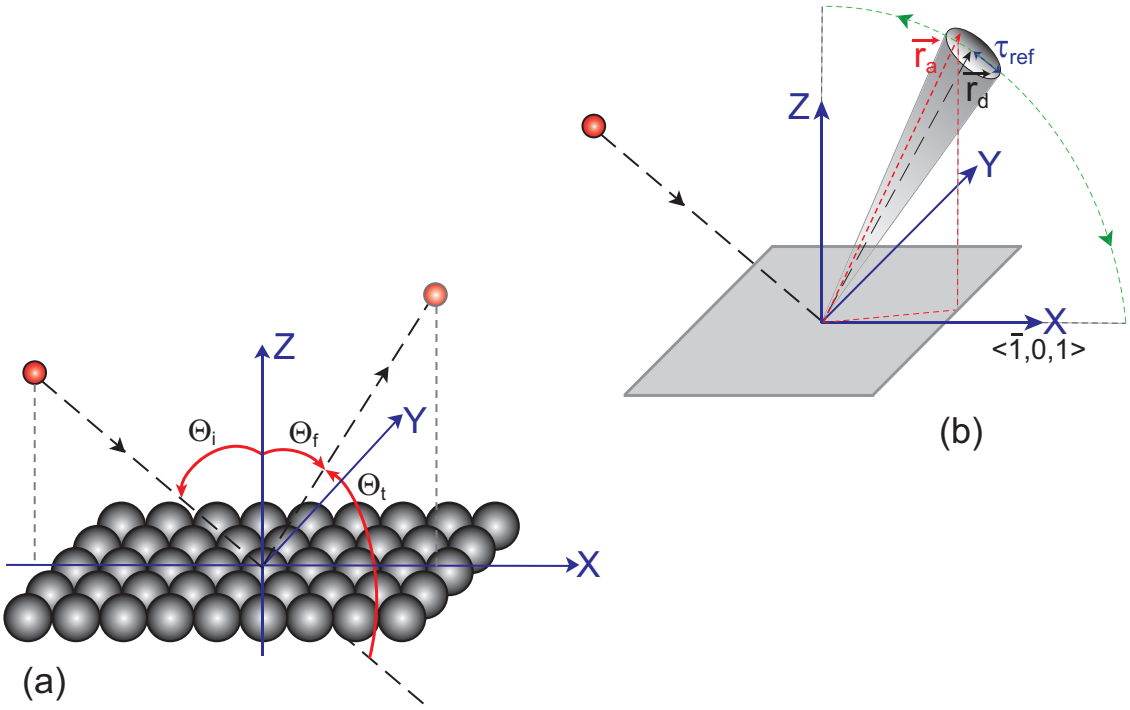

Figure 4: (a) Definition of initial Θ_i and final Θ_f polar angles for N atoms scattered off Ag(111). The (in-plane) total scattering angle, which is defined as $\Theta_t = 180^\circ - (\Theta_i + \Theta_f)$, is also shown. (b) Schematic representation of the model used to account for our results per solid angle. $\overrightarrow{r_d}$ and $\overrightarrow{r_a}$ are, respectively, the vector positions of the experimental detector and of a reflected atom that is selected. τ_{ref} is the acceptance angle as defined in the text.

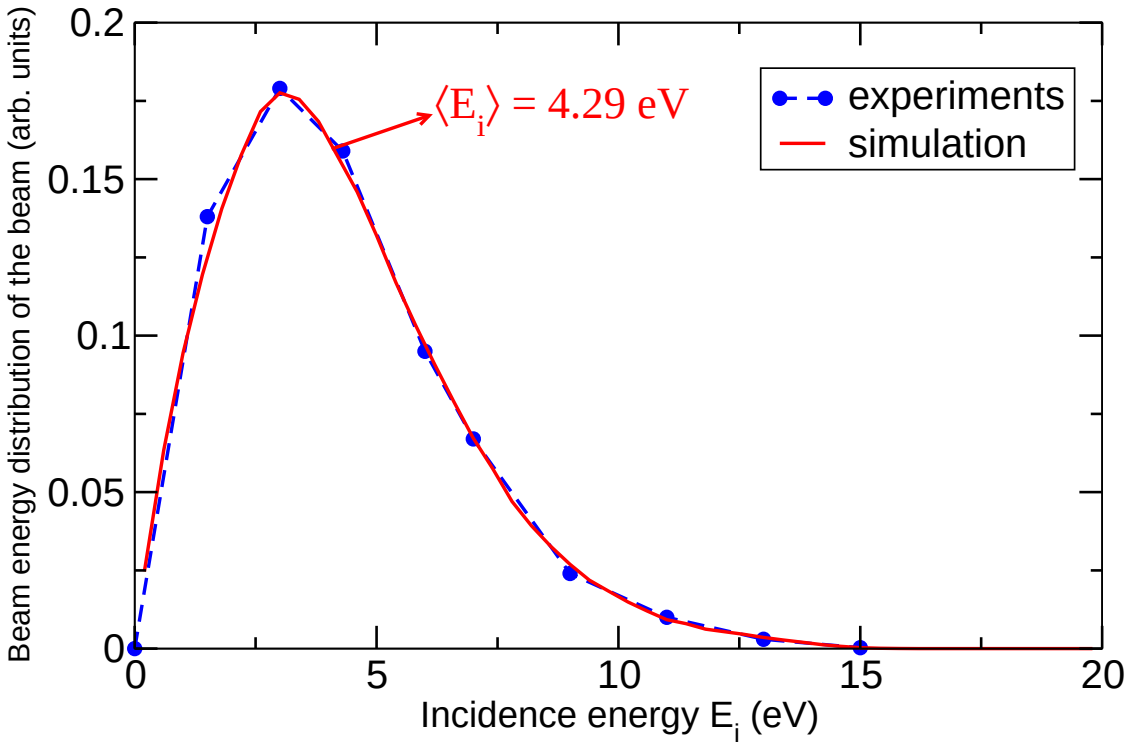

Figure 5: Beam energy distribution used in the experiments[36] and reproduced in this work with a Metropolis algorithm using 600000 iterations. The average energy obtained is: $\langle E_i \rangle = 4.29$ eV which compares very well to the experimental one of about 4.3 eV.

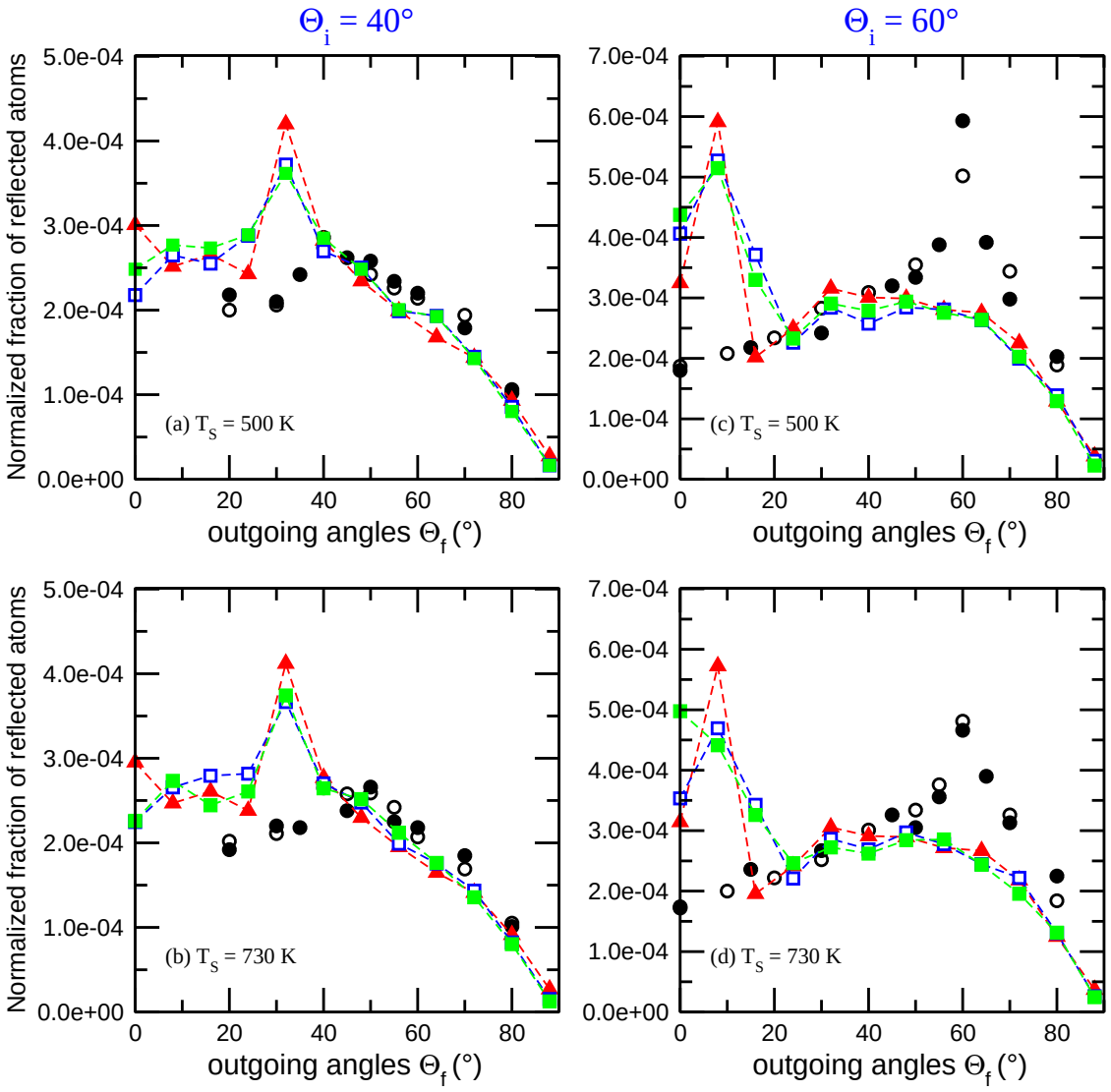

Figure 6: Angular distributions for in-plane scattering of N on Ag(111) at $\Theta_i = 40^\circ$ (left panels a-b) and $\Theta_i = 60^\circ$ (right panels c-d). The surface temperature is: 500 K in (a),(c) and 730 K in (b),(d). Our results are obtained for a monoenergetic beam (initial kinetic energy E_i^T of 4.3 eV) using three kinds of simulation: adiabatic model (red filled triangles), GLO model (blue open squares) and LDFA+GLO (green filled squares). All the results are normalized to the experimental data[36] (open and filled circles representing two independent data set).

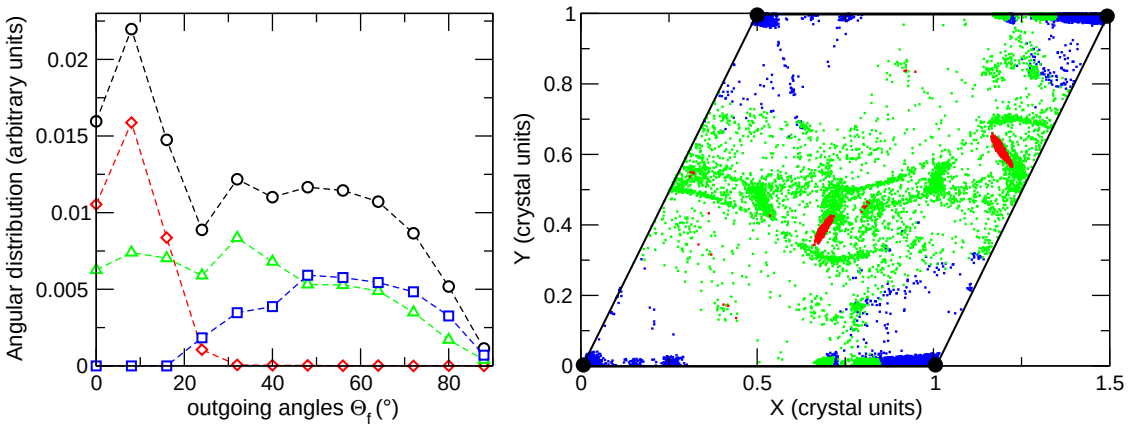

Figure 7: Decomposition of the angular distribution obtained with the GLO model at $\Theta_i = 60°$ and $T_S = 500$ K (cf. Figure 6(c)) as a function of the minimum distance Z_{ref} reached by N atoms (left panel). Black curve: total distribution, red curve: reflection for $Z_{ref} \leq 0.85$ Å, green curve: reflection for $0.85 < Z_{ref} \leq 1.45$ Å, blue curve: reflection for $Z_{ref} > 1.45$ Å. The same decomposition is applied in the right panel for the (X,Y) distribution at Z_{ref} of N atoms over the surface unit cell. The unit cell is represented by black lines whereas black circles stand for first layer Ag atoms. For clarity, all points have been merged into the surface unit cell.

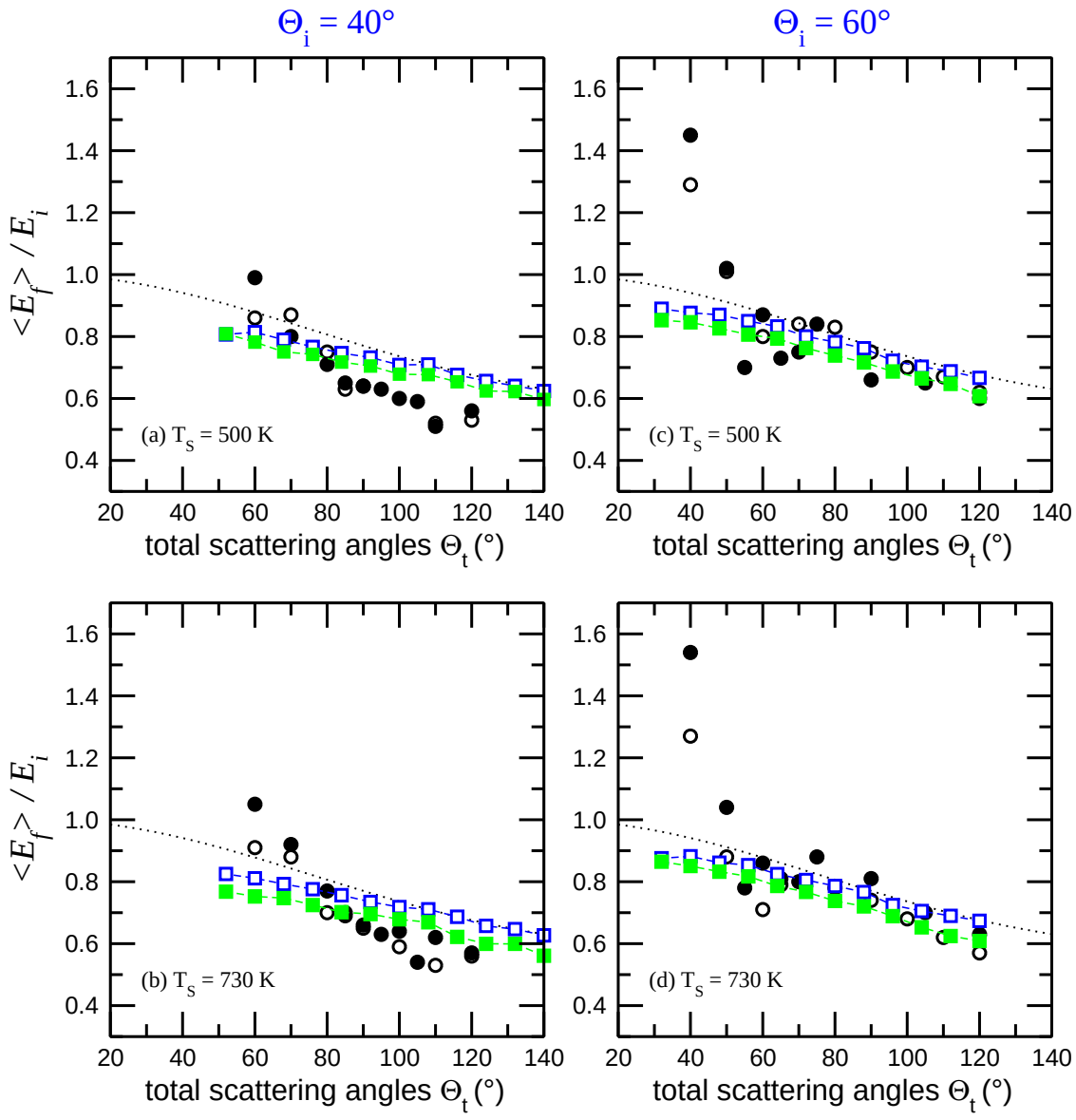

Figure 8: Ratio of final to initial energy as a function of the total scattering angle ($\Theta_t = 180 - (\Theta_i + \Theta_f)$) for N scattered off Ag(111). Our simulation results are obtained for a monoenergetic beam (initial kinetic energy E_i^T of 4.3 eV) and are represented by blue open squares (GLO) and green filled squares (LDFA+GLO). The experimental results,[36] shown for two independent data sets, are depicted by open and filled circles. The result obtained with a hard-sphere model is also shown (black dotted lines).

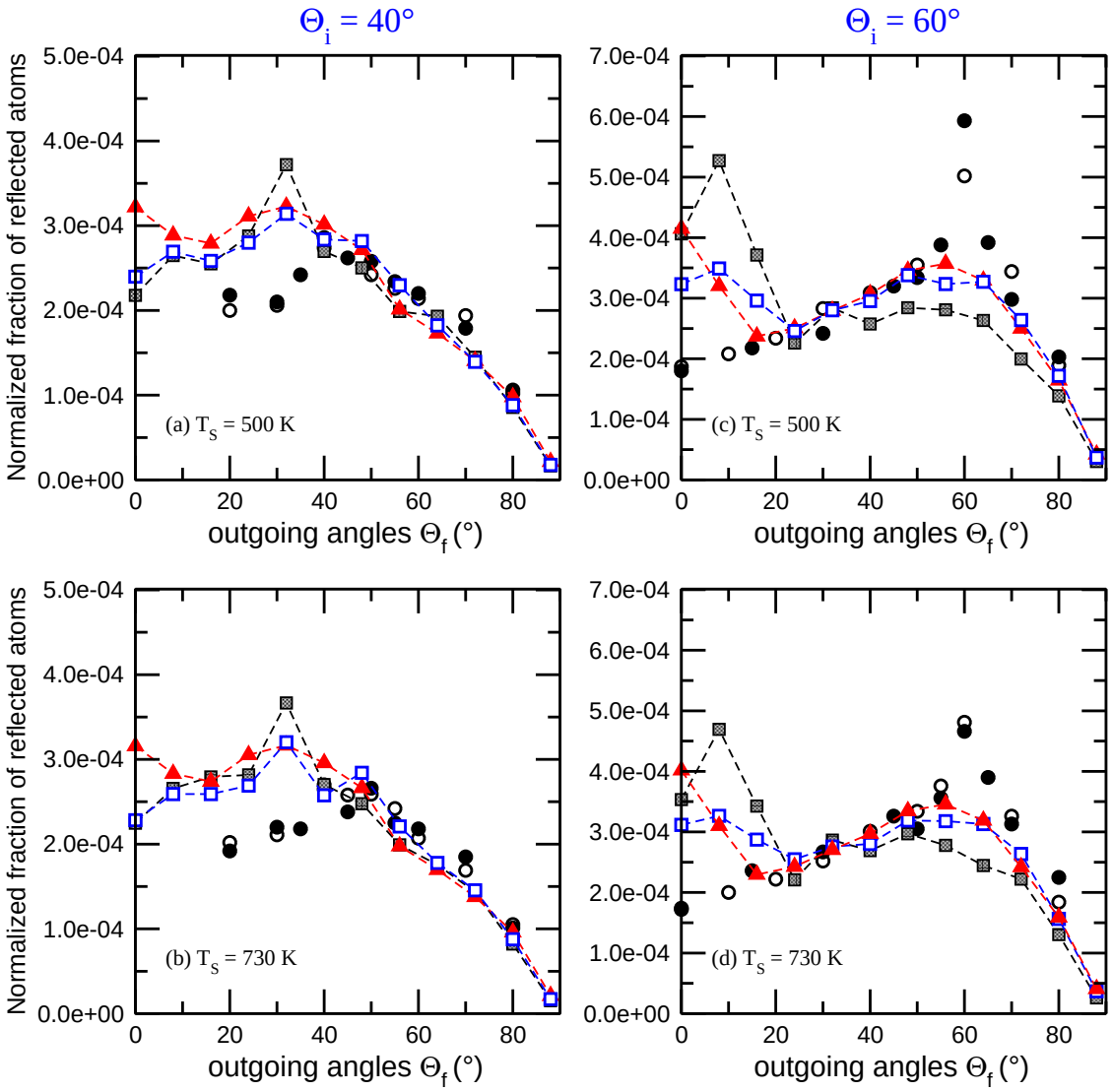

Figure 9: Angular distributions for in-plane scattering of N on Ag(111) at $\Theta_i = 40^\circ$ (left panels) and $\Theta_i = 60^\circ$ (right panels). The surface temperature is: 500 K in (a),(c) and 730 K in (b),(d). Our results are obtained for an effusive beam (initial average kinetic energy $\langle E_i^T \rangle$ of about 4.3 eV) using two kinds of simulations: adiabatic model (red filled triangles) and GLO model (blue open squares). All the results are normalized to the experimental data[36] (open and filled circles representing two independent data set). The results obtained with the GLO model and a monoenergetic beam are also shown for comparison (black squares).

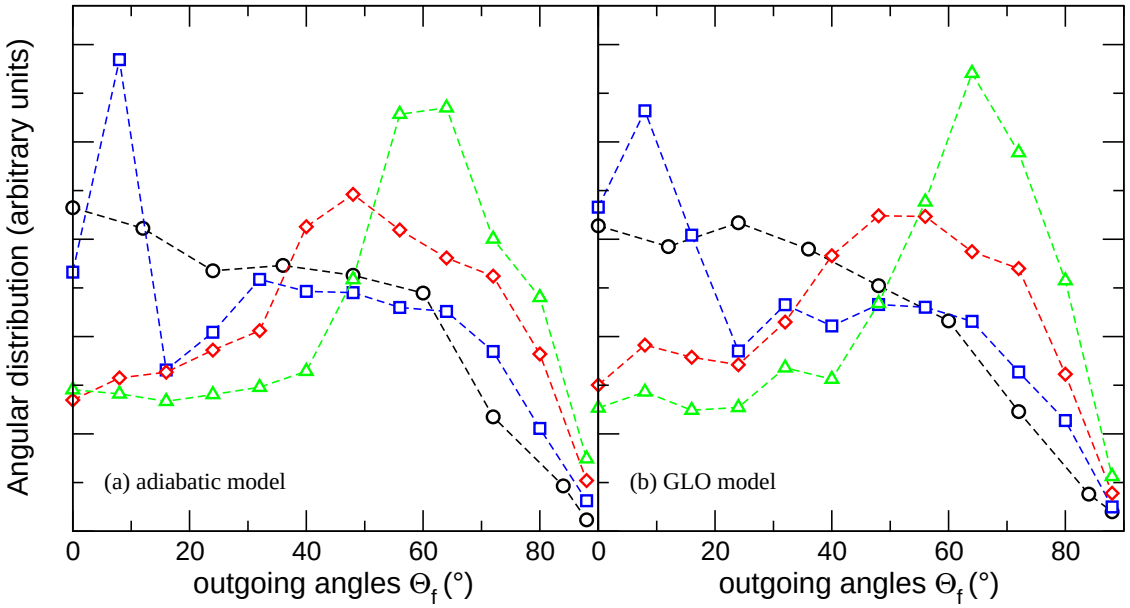

Figure 10: Angular distributions for in-plane scattered N atoms off Ag(111) at $\Theta_i = 60^\circ$ obtained with the adiabatic model (left panel) and the GLO model (right panel). Various initial kinetic energies E_i^T have been considered: 1.0 eV (black circles), 4.3 eV (blue squares), 6.0 eV (red diamond) and 10.0 eV (green triangles). Surface temperature is 500 K for the GLO model.

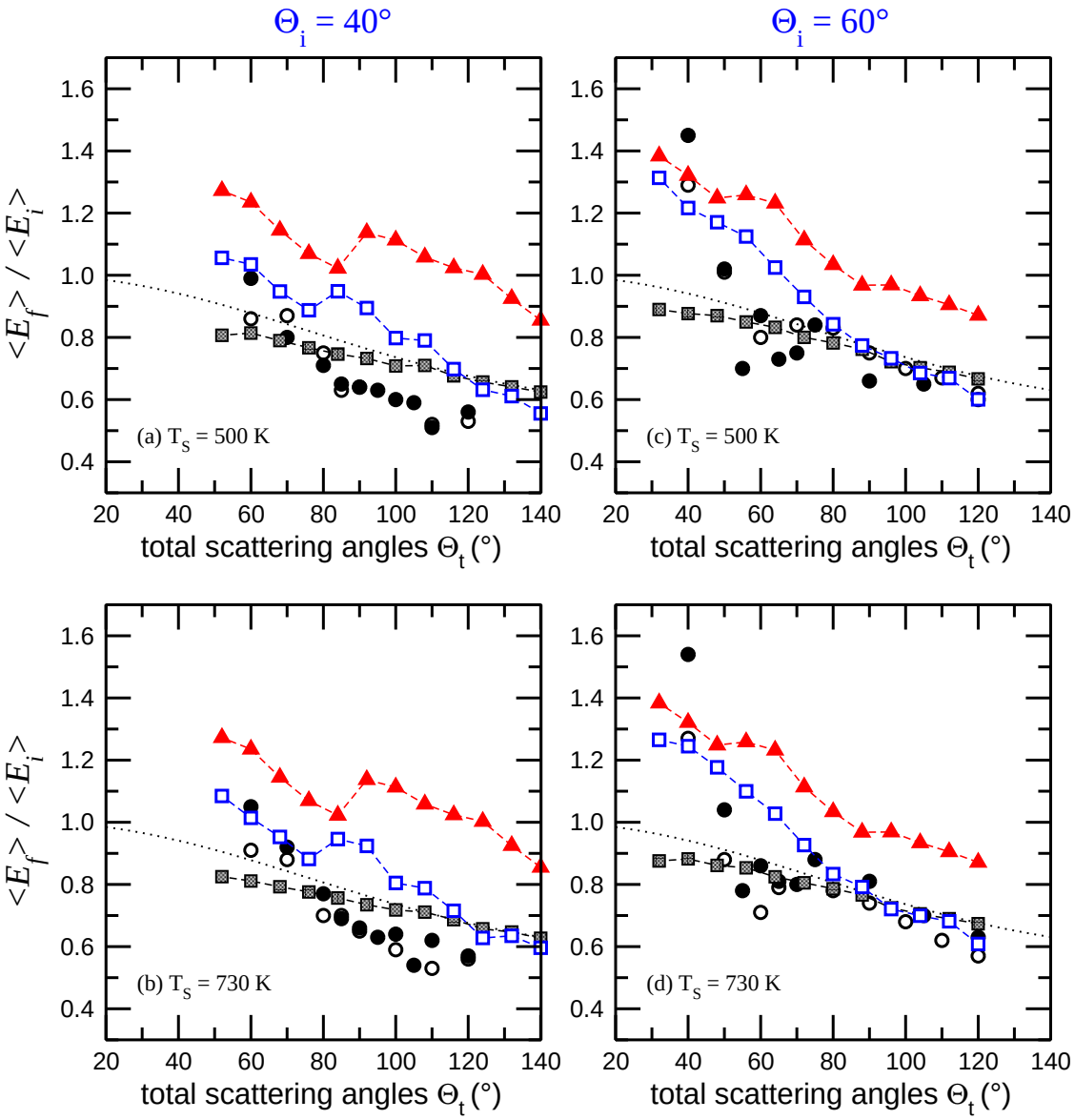

Figure 11: Ratio of final to initial energy as a function of the total scattering angle ($\Theta_t = 180 - (\Theta_i + \Theta_f)$) for N atoms scattered off Ag(111). Our simulation results are obtained for an effusive beam (initial average kinetic energy $\langle E_i^T \rangle$ of about 4.3 eV) and are represented by red filled triangles (adiabatic) and blue open squares (GLO). The experimental results,[36] shown for two independent data sets, are depicted by open and filled circles. The results obtained with the GLO model and for a monoenergetic beam are also shown for comparison (black squares). Black dotted lines represent the result obtained with a hard-sphere model.